

## **GAS-SURFACE INTERACTION EFFECT ON SHOCK-DETACHMENT DISTANCE OF POWER-LAW LEADING EDGES IN HYPERSONIC AIRFLOW**

**Wilson F. N. Santos**

*wilson@lcp.inpe.br*

Combustion and Propulsion Laboratory, National Institute for Space Research, Cachoeira Paulista, SP, 12630-000, Brazil

***Abstract.** This work deals with a numerical study of power-law leading edges situated in a rarefied hypersonic flow. The primary aim of this paper is to examine the effect of partial surface accommodation on the shock wave structure. Partial surface accommodation effects on the shock wave structure have been investigated by employing the Direct Simulation Monte Carlo (DSMC) method in combination with the Cercignani-Lampis-Lord gas-surface interaction model, which incorporates separate accommodation coefficients for normal and tangential velocity components. The work is motivated by interest in investigating the shock wave structure of power-law shaped leading edges as possible candidates for blunting geometry of hypersonic leading edges. The sensitivity of shock wave shape, shock standoff distance, and shock thickness is calculated by using a model that classifies the molecules in three distinct classes: “undisturbed freestream”, “reflected from the boundary” and “scattered”, i.e., molecules that had been indirectly affected by the presence of the leading edge. The analysis shows significant differences on the shock wave structure due to variations on the normal and tangential accommodation coefficients.*

***Keywords:** Hypersonic flow, Rarefied flow, DSMC, Power-law shape, Gas-surface interaction*

## **GAS-SURFACE INTERACTION EFFECT ON SHOCK-DETACHMENT DISTANCE OF POWER-LAW LEADING EDGES IN HYPERSONIC AIRFLOW**

**Wilson F. N. Santos**

wilson@lcp.inpe.br

Combustion and Propulsion Laboratory, National Institute for Space Research, Cachoeira  
Paulista, SP, 12630-000, Brazil

**Abstract.** *This work deals with a numerical study of power-law leading edges situated in a rarefied hypersonic flow. The primary aim of this paper is to examine the effect of partial surface accommodation on the shock wave structure. Partial surface accommodation effects on the shock wave structure have been investigated by employing the Direct Simulation Monte Carlo (DSMC) method in combination with the Cercignani-Lampis-Lord gas-surface interaction model, which incorporates separate accommodation coefficients for normal and tangential velocity components. The work is motivated by interest in investigating the shock wave structure of power-law shaped leading edges as possible candidates for blunting geometry of hypersonic leading edges. The sensitivity of shock wave shape, shock standoff distance, and shock thickness is calculated by using a model that classifies the molecules in three distinct classes: “undisturbed freestream”, “reflected from the boundary” and “scattered”, i.e., molecules that had been indirectly affected by the presence of the leading edge. The analysis shows significant differences on the shock wave structure due to variations on the normal and tangential accommodation coefficients.*

**Keywords:** *Hypersonic flow, Rarefied flow, DSMC, Power-law shape, Gas-surface interaction*

### **1. INTRODUCTION**

In typical aerospace missions, vehicle performance is directly related to the aerodynamic characteristics of the design. In particular, the lift-drag (L/D) ratio indicates one aspect of the aerodynamic efficiency of the vehicle. One class of aerospace vehicle that has shown the ability to attain a higher L/D ratio compared to the conventional designs is waveriders (Nonweiler, 1959). Waveriders are designed analytically with infinitely sharp leading edge for shock wave attachment. The potential for high L/D ratio on waveriders originates from the high-pressure region between the shock wave and the lower surface. Due to the sharp leading edge, the attached shock wave prevents the high-pressure gas from the lower surface to communicate with the gas on the upper surface. However, as any practical waverider will have some degree of leading edge bluntness for heat transfer, manufacturing and handling concerns, then the predicted performance of waverider configurations may not be achieved. Moreover, because of the viscous effects, the shock wave will be detached from the leading edge and, hence, the aerodynamic performance of the vehicle may be degraded from ideal performance. Typically, a round leading edge (circular cylinder) with constant radius of curvature near the stagnation point has been chosen. Nevertheless, shock detachment distance on a cylinder, with associated leakage, scales with the radius of curvature.

Certain classes of non-circular shapes may provide the required bluntness with smaller shock separation than round leading edges, thus allowing manufacturing, and ultimately

heating control, with reduced aerodynamic losses.

Power-law shaped leading edges ( $y \propto x^n$ ,  $0 < n < 1$ ) may provide the required bluntness for heat transfer, manufacturing and handling concerns with reduced departures from ideal aerodynamic performance. This concept is based on work of Mason and Lee (1994), who have pointed out, based on Newtonian flow analysis, that power-law shapes exhibit both blunt and sharp aerodynamic properties. They suggested the possibility of a difference between shapes that are geometrically sharp and shapes that behave aerodynamically as if they were sharp.

A great deal of works (Santos and Lewis, 2002a, 2002b, 2003, 2004a, 2004b, 2005 and Santos, 2004a, 2004b and 2005) has been carried out recently on power-law shape representing blunt geometries. The major interest in these works has gone into considering the power-law body as possible candidate for blunting geometries of hypersonic leading edges. Based on recent interest in hypersonic waveriders for high-altitude/low-density applications (Anderson, 1990, Potter and Rockaway, 1994, Rault, 1994, Graves and Argrow, 2001, Shvets et al., 2005), Santos (2004a and 2004b) has investigated the effect of the power-law exponent on the shock wave structure over these leading edges. Nevertheless, those works (Santos, 2004a and 2004b) has been concentrated primarily on the analysis of the flowfield structure by considering the diffuse reflection model as being the gas-surface interaction. Nonetheless, as a space flight vehicle is exposed to a rarefied environment over a considerable time, a departure from fully diffuse model is observed, resulting from the colliding molecules that clean the surface of the vehicle, which becomes gradually decontaminated. Molecules reflected from clean surfaces show lobular distribution in direction. The flux distribution of scattered molecules emitted from clean surfaces frequently has a lobular shape that is centered about an angle that tends to approach the specular angle for very high energies and/or low angle of attack.

In this scenario, the emphasis of this work is to assess the sensitivity of the shock standoff distance, shock wave thickness and shock wave shape to variations on surface accommodation coefficient. For the high altitude/high Knudsen number of interest ( $Kn > 0.1$ ), the flowfield is sufficiently rarefied that continuum method becomes inappropriate. Alternatively, the DSMC method is used in the current study to calculate the rarefied hypersonic two-dimensional flow on the leading edge shapes.

## 2. GAS-SURFACE INTERACTION MODEL

The DSMC method (Bird, 1994) has proved to be an extremely useful and flexible tool in the analysis of rarefied hypersonic non-equilibrium gas flows. The reliability of the method is entirely dependent on the accuracy of the collision models used to simulate particles interactions. As the majority of the practical problems involve gas-surface interaction phenomena, a suitable boundary condition is required in order to obtain reliable results from numerical simulation of rarefied gas flows.

The majority of DSMC codes so far developed has made the assumption of complete diffuse particle reflection or has used the Maxwell model. Originally, Maxwell (1879) speculated that a fraction  $\phi$  of the incident molecules would adhere to the surface long enough to come to thermal equilibrium with the surface and would be reflected in a diffuse manner, and the remaining fraction  $(1-\phi)$  would be reflected specularly. In a specular reflection model, molecules are reflected like a perfectly elastic sphere with reversal of the normal component of velocity and no change in either the parallel component of velocities and energy. In a diffuse reflection model, molecules are reflected equally in all directions usually with a complete thermal accommodation. The final velocity of the molecules is randomly assigned according to a half-range Maxwellian distribution determined by the wall temperature.

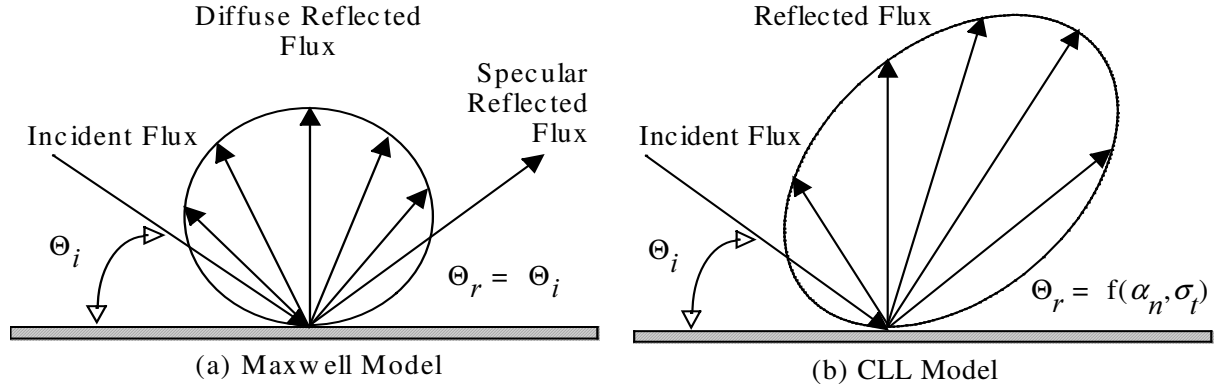


Figure 1: Drawing illustrating (a) the Maxwell reflection model and (b) the CLL reflection model.

The Maxwell model was followed by the introduction of three accommodation coefficients that describe the degree of accommodation of the incident normal momentum, tangential momentum and kinetic energy to those of the surface. The traditional definition (Schaaf and Chambre, 1961) for these coefficients is usually expressed as being,

$$\sigma_n = \frac{p_i - p_r}{p_i - p_w} \quad \sigma_t = \frac{\tau_i - \tau_r}{\tau_i} \quad \alpha = \frac{e_i - e_r}{e_i - e_w} \quad (1)$$

where terms  $p$ ,  $\tau$  and  $e$  refer to the momentum flux acting normal and tangential to the surface, and the energy flux to the surface per unit area per unit time, respectively; subscripts  $i$  and  $r$  stand for the incident and reflected components, and  $w$  refers to the component that would be produced by a diffuse reflection at the temperature of the surface.

Data from many experiments show that molecules reflected or re-emitted from solid surfaces present lobular distributions under high vacuum conditions and are poorly represented by the Maxwell model. Nevertheless, this model is widely used because it satisfies the principle of detailed balance or reciprocity. Detailed balance means that at equilibrium every molecular process and its inverse process must individually balance.

A phenomenological model that satisfies detailed balance and has demonstrated improvement over the Maxwell model has been proposed by Cercignani and Lampis (1971) (CL model). This model is based on the definition of the accommodation coefficients  $\alpha_n$  and  $\alpha_t$  that represent the accommodation coefficients for the kinetic energy associated with the normal and tangential components of velocity. The CL model provides a continuous spectrum of behavior from specular reflection at one end to diffuse reflection with complete energy accommodation at the other, and produces physically realistic distributions of direction and energy re-emitted molecules. Lord (1991a) has shown that the CL model is suited for the DSMC method, and described how to incorporate it into the DSMC method. The DSMC method with Lord's implementation is referred as the Cercignani-Lampis-Lord (CLL) method. Figure 1 displays a schematic comparison of the Maxwell reflection model and the CLL reflection model. The CL model has also been extended for covering diffuse scattering with partial energy accommodation and for simulating the accommodation of vibrational energy of a diatomic molecule modeled as simple harmonic oscillator (Lord, 1991b) and an anharmonic oscillator (Lord, 1995).

In order to simulate the partial surface accommodation, the CLL model (Lord, 1991a) was included in this DSMC calculation. The CLL model is derived by assuming that there is no coupling between the normal and tangential momentum components. The two adjustable

parameters appearing in the CLL model are the normal component of translational energy  $\alpha_n$  and the tangential component of momentum  $\sigma_t$ . However, in the implementation of the CLL model into the DSMC method, Bird (1994) has shown that it is equivalent to specify the normal  $\alpha_n$  and tangential  $\alpha_t$  components of translational energy, since  $\alpha_t = \sigma_t (2 - \sigma_t)$ , and thus that  $\sigma_t < \alpha_t$ , assuming that  $\sigma_t$  lies between 0 and 1. In the present simulations,  $\alpha_n$  and  $\sigma_t$  are used as being the two adjustable parameters. It is important to mention that in the CLL model the accommodation of internal energy is allowed to be independent of the translational accommodation.

### 3. LEADING-EDGE GEOMETRY

In dimensional form, the body power-law shapes are given by the following expression,

$$y = ax^n \quad (2)$$

where  $n$  is the power-law exponent and  $a$  is the power-law constant which is a function of  $n$ .

The power-law shapes are modeled by assuming a sharp leading edge of half angle  $\theta$  with a circular cylinder of radius  $R$  inscribed tangent to this wedge. The power-law shapes, inscribed between the wedge and the cylinder, are also tangent to them at the same common point where they have the same slope angle. The circular cylinder diameter provides a reference for the amount of blunting desired on the leading edges. It was assumed a leading edge half angle of 10 degree, a circular cylinder diameter of  $10^{-2}$ m and power-law exponents of 1/2, 2/3, and 3/4. Figure 2(a) illustrates schematically this construction for the set of power-law leading edges investigated.

From geometric considerations, the power-law constant  $a$  is obtained by matching slope on the wedge, circular cylinder and power-law body at the tangency point. The common body height  $H$  at the tangency point is equal to  $2R\cos\theta$ , and the body length  $L$  from the nose to the tangency point in the axis of symmetry is given by  $nH/2\tan\theta$ . It was assumed that the power-law leading edges are infinitely long but only the length  $L$  is considered since the wake region behind the power-law bodies is not of interest in this investigation.

### 4. COMPUTATIONAL TOOL

In this study, the particle simulations were performed by using the DSMC method developed by Bird (1994). The DSMC method simulates fluid flow by using thousands to millions of particles. These particles are tracked as they move, collide and undergo boundary interactions in simulated physical space. In addition, particle motions are assumed to be decoupled from particle collisions and each process is computed independently during a time step used to advance the simulation. This time step must be sufficiently small in comparison with the local mean collision time (Garcia and Wagner, 2000, and Hadjiconstantinou, 2000) such that the assumption of decoupled particle motions and collisions is not violated.

The molecular collisions are modeled using the variable hard sphere (VHS) molecular model (Bird, 1981) and the no time counter (NTC) collision sampling technique (Bird, 1989). The VHS model employs the simple hard sphere angular scattering law so that all directions are equally possible for post-collision velocity in the center-of-mass frame of reference. However, the collision cross section is a function of the relative energy in the collision. The energy exchange between kinetic and internal modes is controlled by the Borgnakke-Larsen statistical model (Borgnakke and Larsen, 1975). Simulations are performed using a non-reacting gas model consisting of two chemical species,  $N_2$  and  $O_2$ . Energy exchanges between

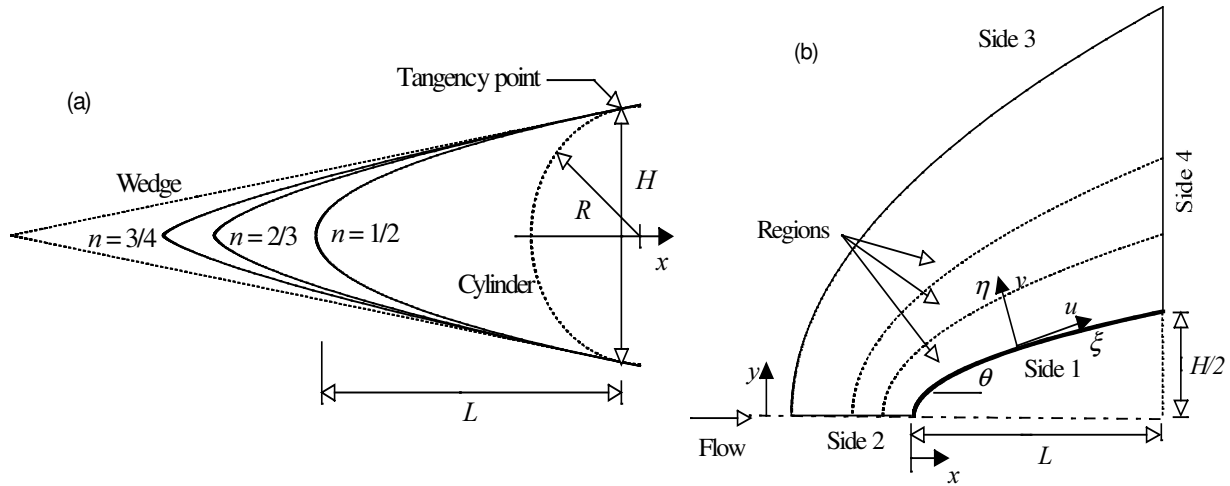


Figure 2: Drawing illustrating (a) the leading edge shapes and (b) the computational domain.

the translational and internal modes are considered. For this study, the relaxation numbers of 5 and 50 were used for the rotation and vibration, respectively.

## 5. COMPUTATIONAL FLOW DOMAIN AND GRID

The computational domain is made large enough so that the upstream and side boundaries can be specified as freestream conditions. Figure 2(b) depicts the physical extent of the computational domain for the present simulations. Advantage of the flow symmetry is taken into account, and molecular simulation is applied to one-half of a full configuration. The computational domain is divided into an arbitrary number of regions, which are subdivided into computational cells. The cells are further subdivided into four subcells, two subcells/cell in each coordinate direction. The linear dimensions of the cells should be small in comparison with the scale length of the macroscopic flow gradients normal to the streamwise directions, which means that the cell dimensions should be of the order of or even smaller than the local mean free path (Alexander et al., 1998 and 2000). In the current DSMC code, the cell provides a convenient reference for the sampling of the macroscopic gas properties, while the collision partners are selected from the same subcell. As a result, the flow resolution is much higher than the cell resolution.

Referring to Fig. 2(b), side 1 is defined by the body surface. Reflection with incomplete surface accommodation is the condition applied to this side. Side 2 is a plane of symmetry, where all flow gradients normal to the plane are zero. At the molecular level, this plane is equivalent to a specular reflecting boundary. Side 3 is the freestream side through which simulated molecules enter and exit. Finally, the flow at the downstream outflow boundary, side 4, is predominantly supersonic and vacuum condition is specified (Guo and Liaw, 2001). At this boundary, simulated molecules can only exit.

Numerical accuracy in DSMC method depends on the grid resolution chosen as well as on the number of particles per computational cell. Both effects were investigated to determine the number of cells and the number of particles required to achieve grid independence solutions.

The grid generation scheme used in this study follows that procedure presented by Bird (1994). Along the outer boundary (side 3) and the body surface (side 1) (see Fig. 2(b)), point distributions are generated in such way that the number of points on each side is the same ( $\xi$ -direction in Fig. 2(b)). Then, the cell structure is defined by joining the corresponding points on each side by straight lines and then dividing each of these lines into segments which are

joined to form the system of quadrilateral cells ( $\eta$ -direction in Fig. 2(b)). The distribution can be controlled by a number of different distribution functions that allow the concentration of points in regions where high flow gradients or small mean free paths are expected.

A grid independence study was made with three different structured meshes in each coordinate direction. The effect of altering the cell size in the  $\xi$ -direction was investigated with grids of 35(coarse), 70(standard) and 105(fine) cells, and 50 cells in the  $\eta$ -direction for power-law exponent of 1/2. In analogous fashion, an examination was made in the  $\eta$ -direction with grids of 25(coarse), 50(standard) and 75(fine) cells, and 70 cells in the  $\xi$ -direction for power-law exponent of 1/2. Each grid was made up of non-uniform cell spacing in both directions. The effect (not shown) of changing the cell size in both directions on the heat transfer, pressure and skin friction coefficients was rather insensitive to the range of cell spacing considered, indicating that the standard grid, 70x50 cells, for power-law exponent of 1/2, is essentially grid independent. A similar procedure was performed for the two other cases investigated. Results indicated that a grid of 80x50 and 90x50 for power-law exponents of 2/3 and 3/4 respectively, were considered fully independent. Of particular interest is the number of cells in the  $\eta$ -direction for the three power-law cases investigated. It should be emphasized that, even though the number of cells is the same, the computational domain size is different for each one of the cases; side 2 shown in Fig. 2(b) corresponds to 8, 6 and  $5\lambda_\infty$  for power-law exponents of 1/2, 2/3 and 3/4, respectively.

In a second stage of the grid independence investigation, a similar examination was made for the number of molecules. The standard grid for power-law exponent of 1/2, 70x50 cells, corresponds to, on average, a total of 121,000 molecules. Two new cases using the same grid, corresponding to 108,000 and 161,000 molecules in the entire computational domain, were investigated. As the three cases presented approximately the same results (see Santos and Lewis, 2005) for the heat transfer, pressure and skin friction coefficients, then the standard grid with a total of 121,000 molecules is enough for the computation of the aerodynamic surface quantities.

## 6. FREESTREAM AND FLOW CONDITIONS

The freestream and flow conditions used in the present calculations are those given by Santos (2004a) and summarized in Tab. 1. The gas properties considered in the simulation are those given by Bird (1994) and tabulated in Tab. 2. Referring to Tabs. 1 and 2,  $T_\infty$ ,  $p_\infty$ ,  $\rho_\infty$ ,  $n_\infty$ ,  $\mu_\infty$ , and  $\lambda_\infty$  stand respectively for temperature, pressure, density, number density, viscosity and mean free path, and  $X$ ,  $m$ ,  $d$  and  $\omega$  account respectively for mole fraction, molecular mass, molecular diameter and viscosity index.

Table 1: Freestream Conditions

$T_\infty$ (K)	$p_\infty$ (N/m <sup>2</sup> )	$\rho_\infty$ (kg/m <sup>3</sup> )	$n_\infty$ (m <sup>-3</sup> )	$\mu_\infty$ (Ns/m <sup>2</sup> )	$\lambda_\infty$ (m)	$V_\infty$ (m/s)
220.0	5.582	$8.753 \times 10^{-5}$	$1.8209 \times 10^{21}$	$1.455 \times 10^{-5}$	$9.03 \times 10^{-4}$	3560

Table 2: Gas Properties

	$X$	$m$ (kg)	$d$ (m)	$\omega$
O <sub>2</sub>	0.237	$5.312 \times 10^{-26}$	$4.01 \times 10^{-10}$	0.77
N <sub>2</sub>	0.763	$4.65 \times 10^{-26}$	$4.11 \times 10^{-10}$	0.74

The freestream velocity  $V_\infty$ , assumed to be constant at 3.56 km/s, corresponds to a freestream Mach number  $M_\infty$  of 12. The wall temperature  $T_w$  is assumed constant at 880 K, which corresponds to 4 times the freestream temperature.

The overall Knudsen number  $Kn_\infty$ , defined as the ratio of the freestream mean free path  $\lambda_\infty$  to the diameter of the circular cylinder, corresponds to 0.09. The Reynolds number per unit of meter is  $Re_\infty = 21416.3$ , also based on conditions in the undisturbed stream.

In order to simulate the incomplete surface accommodation, the CLL model implemented into the DSMC code considered only the normal and tangential accommodation coefficients. The internal energy accommodation was kept equal to one for all calculations presented in this work. Hence,  $\alpha_n$  and  $\sigma_t$  are used as being the two adjustable parameters. The DSMC calculations were performed independently for three distinct numerical values for  $\alpha_n$  and  $\sigma_t$ : 0.6, 0.8 and 1. It is important to mention that  $\alpha_n$  and  $\sigma_t$  equal to 1 represent the diffusion reflection case.

## 7. COMPUTATIONAL PROCEDURE

The problem of predicting the shape and location of detached shock waves has been stimulated by the necessity for blunt noses and leading edges configurations designed for hypersonic flight in order to cope with the aerodynamic heating. In addition, the ability to predict the shape and location of shock waves is of primary importance in analysis of aerodynamic interference. Furthermore, the knowledge of the shock wave displacement is especially important in waveriders (Nonweiler, 1959), since these hypersonic configurations usually rely on shock wave attachment at the leading edges to achieve their high L/D ratio at high-lift coefficient.

In this present account, the shock wave structure, defined by shape, thickness and detachment of the shock wave, is predicted by employing a procedure based on the physics of the particles. In this respect, the flow is assumed to consist of three distinct classes of molecules; class I molecules denote those molecules from freestream that have not been affected by the presence of the leading edge; class II molecules designate those molecules that, at some time in their past history, have struck and been reflected from the body surface; and finally, class III molecules define those molecules that have been indirectly affected by the presence of the body. Figure 3(a) illustrates the definition for the molecular classes.

It is assumed that the class I molecule changes to class III molecule when it collides with class II or class III molecule. Class I or class III molecule is progressively transformed into class II molecule when it interacts with the body surface. Also, a class II molecule remains class II regardless of subsequent collisions and interactions. Hence, the transition from class I molecules to class III molecules may represent the shock wave, and the transition from class III to class II may define the boundary layer.

A typical distribution of class III molecules along the stagnation streamline for blunt leading edges is displayed in Fig. 3(b) along with the definition used to determine the thickness, displacement and shape of the shock wave. In this figure,  $X$  is the distance  $x$  along the stagnation streamline (see Fig. 2(b)), normalized by the freestream mean free path  $\lambda_\infty$ , and  $f_{III}$  is the number of molecules for class III to the total amount of molecules inside each cell.

In a rarefied flow, the shock wave has a finite region that depends on the transport properties of the gas, and it can no longer be considered as a discontinuity obeying the classical Rankine-Hugoniot relations. In this context, the shock standoff distance  $\Delta$  is defined as being the distance between the shock wave center and the nose of the leading edge along the stagnation streamline. As shown in Fig. 3(b), the center of the shock wave is defined by the station that corresponds to the maximum value for  $f_{III}$ . The shock wave thickness  $\delta$  is defined by the distance between the stations that correspond to the mean value for  $f_{III}$ . Finally,

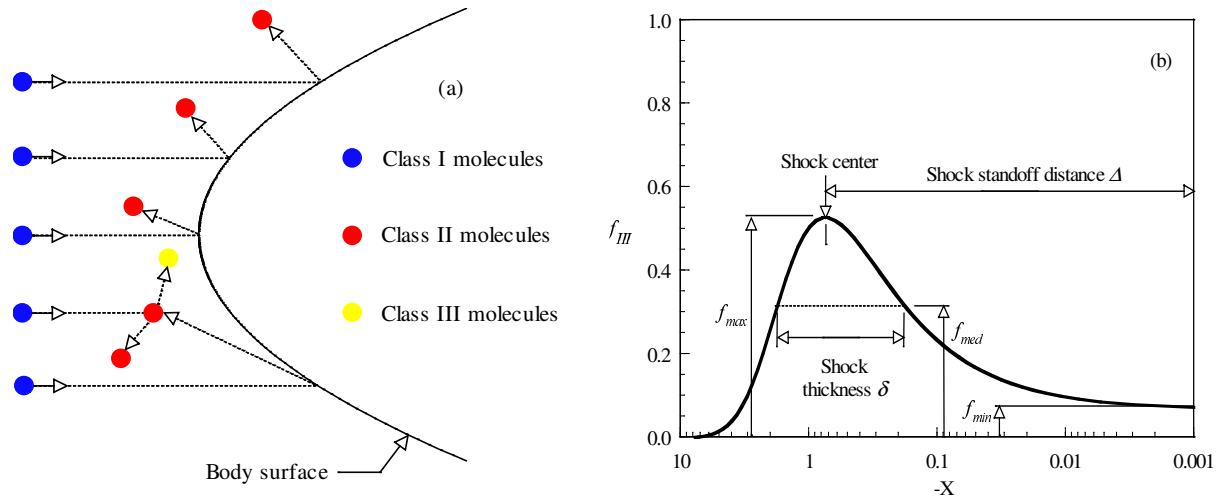


Figure 3: (a) Drawing illustrating the classification of molecules and (b) Schematic of shock wave structure.

the shock wave shape (shock wave “location”) is determined by the coordinate points given by the maximum value in the  $f_{III}$  distribution along the lines departing from the body surface, i.e.,  $\eta$ -direction as shown in Fig. 2(b).

## 8. COMPUTATIONAL RESULTS AND DISCUSSION

This section focuses on the effects that take place on the shock wave structure due to variations on the leading edge shape and on the surface accommodation coefficients. In this scenario, the purpose of this section is to discuss and to compare differences in the thickness, displacement, and shape of the shock wave due to variations on the power-law exponent  $n$  and on the coefficients  $\alpha_n$  and  $\sigma_t$ . Nevertheless, having computed molecular class properties over a wide range of simulation parameters, it proves instructive to summarize first the major features of the results related to the class of molecules.

### 8.1 Molecular class distribution

The distribution of molecules for the three classes along the stagnation streamline is illustrated in Figs. 4 and 5 for leading edges corresponding to power-law exponents of 1/2 and 3/4. Figures 4(a) and 5(a) display the distribution of molecules for normal accommodation coefficient  $\alpha_n$  of 0.6 and 1 and Figs. 4(b) and 5(b) for the tangential accommodation coefficient  $\sigma_t$  of 0.6 and 1. It is important to note that  $\alpha_n = 1 = \sigma_t$  represent the diffuse reflection case (Santos, 2004a). In addition, in this set of plots,  $f_I$ ,  $f_{II}$  and  $f_{III}$  are the ratio of the number of molecules for class I, II and III, respectively, to the total amount of molecules inside each cell along the stagnation streamline. The class distributions for the power-law exponent of 2/3 are intermediate to these two cases and, therefore, they will not be shown.

By examining Figs. 4 and 5, it is clearly seen that partial accommodation coefficient affects the shock wave structure for this particular group of sharp and blunt leading edges. Consequently, changes in the normal and tangential accommodation coefficients will affect the shape, thickness and displacement of the shock wave in a different manner.

Of great significance in the plots shown in Figs. 4 and 5 is the behavior of the class I molecules for sharp and blunt leading edges. It should be observed in Fig. 5 that molecules from freestream, represented by class I molecules, collide with the nose of the leading edges even after the establishment of the steady state. This represents a sharp leading edge case. In

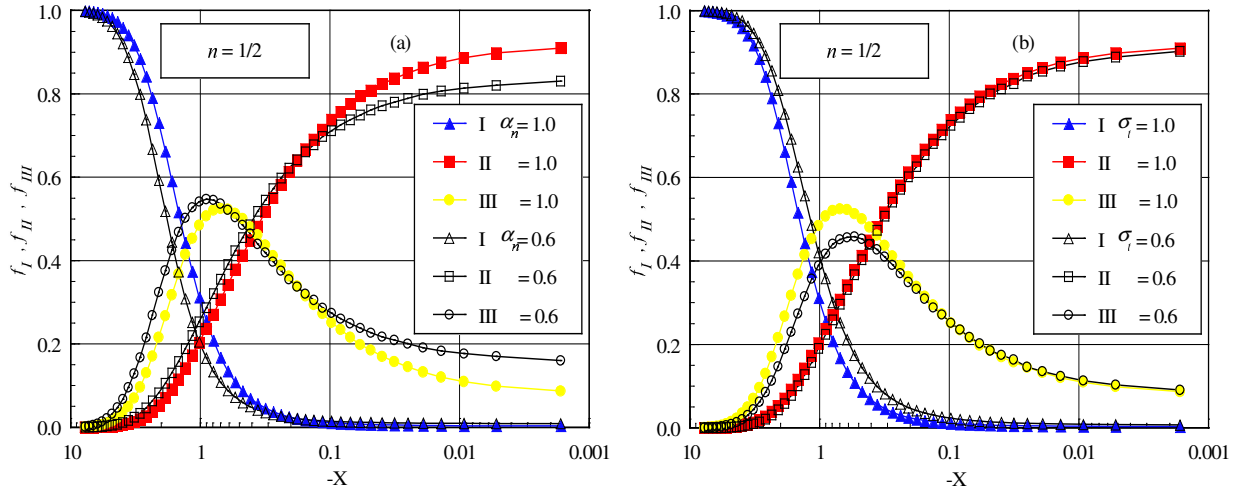


Figure 4: Distributions of molecules for classes I, II and III along the stagnation streamline for power-law exponent of 1/2 and (a)  $\alpha_n$  of 0.6 and (b)  $\sigma_t$  of 0.6.

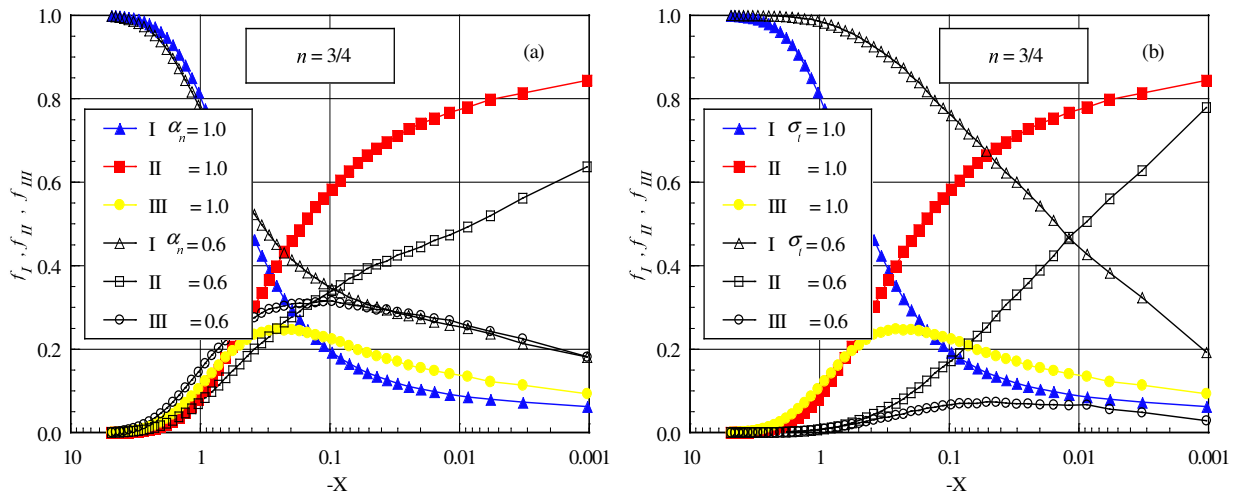


Figure 5: Distributions of molecules for classes I, II and III along the stagnation streamline for power-law exponent of 3/4 and (a)  $\alpha_n$  of 0.6 and (b)  $\sigma_t$  of 0.6.

contrast, molecules from freestream do not reach the nose of the leading edge for that case illustrated in Fig. 4, which represents a blunt leading edge. This is explained by the fact that density (Santos and Lewis, 2004b) increases much more for blunt leading edges in the stagnation region and reaches its maximum value in the stagnation point. In this connection, the buildup of particle density near the nose of the leading edge acts as a shield for molecules coming from the undisturbed stream.

## 8.2 Shock-wave standoff distance

According to the definition shown in Fig. 3(b), the shock wave standoff distance  $\Delta$  can be observed in Figs. 4 and 5 for the power-law shapes shown. The calculated shock wave standoff distance  $\Delta$ , normalized by the freestream mean free path  $\lambda_\infty$ , is tabulated in Tab. 3 for the cases investigated.

It is apparent from the results on Tab. 3 that there is a discrete shock standoff distance for the cases shown. As would be expected, the shock standoff distance decreases with increasing

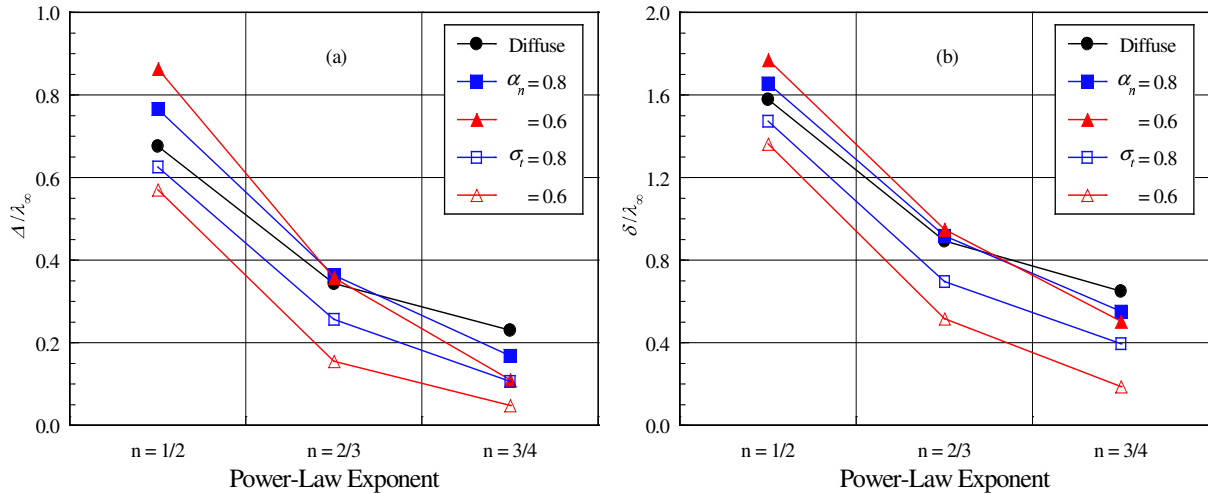


Figure 6: Dimensionless (a) shock standoff distance and (b) shock thickness as a function of the leading edge thickness.

the power-law exponent; as the leading edge becomes sharp. It is also seen that, in general, the shock standoff distance decreases with decreasing the tangential accommodation coefficient and increases by a reduction in the normal accommodation coefficient, even though the shock standoff distance decreased slightly for the sharpest leading edge,  $n = 3/4$ , as the normal accommodation coefficient changed from 1 to 0.6.

For the purpose of visualization, Fig. 6 displays the shock standoff distance, normalized by the freestream mean free path, as a function of the power-law exponent  $n$ .

Table 3: Dimensionless shock wave standoff distance  $\Delta/\lambda_\infty$  for power-law leading edges.

	$n = 1/2$	$n = 2/3$	$n = 3/4$
Diffuse	0.676	0.343	0.230
$\alpha_n = 0.8$	0.766	0.364	0.168
$\alpha_n = 0.6$	0.864	0.358	0.110
$\sigma_t = 0.8$	0.626	0.257	0.106
$\sigma_t = 0.6$	0.570	0.156	0.048

For comparison purpose, the circular cylinder, shown in Fig. 2(a), provides a larger shock detachment, i.e.,  $\Delta/\lambda_\infty$  of 1.65, 1.77 and 1.57 for diffuse,  $\alpha_n = 0.6$  and  $\sigma_t = 0.6$ , respectively. These values are about 2.4, 2.0 and 2.8 times larger than those for  $n = 1/2$ , respectively. The results tend to confirm the expectation that the shock standoff distance for sharp leading edge is smaller than that for blunt leading edge. In fact, the power-law bodies behave as if they had a sharper profile than the representative circular cylinder.

It is important to mention that shock standoff distance becomes important in hypersonic vehicles such as waveriders, which depend on leading edge shock attachment to achieve their high L/D ratio at high lift coefficient. In this connection, the power-law shapes seem to be more appropriate than the circular cylinder, since they present reduced shock wave detachment distances. Nonetheless, smaller shock detachment distance is associated with a higher heat load to the nose of the body. According to Santos and Lewis (2002a), the heat transfer coefficient  $C_{ho}$  ( $= 2q_w/\rho_\infty V_\infty^3$ ) at the stagnation point for power-law bodies defined by power-law exponents of 1/2, 2/3 and 3/4 are 2.4, 2.2 and 1.5 times larger than the heat transfer coefficient for the circular cylinder for the diffuse case. As a result, it should be notice from

this comparison that the ideal blunting leading edge depends on the context. If shock standoff distance is the primary issue in leading edge design of hypersonic waveriders, then power-law leading edges are superior to round leading edges (circular cylinder). In contrast, if the stagnation point heating is the important parameter in the hypersonic vehicle design, then round shapes seem to be superior to the power-law shapes.

### 8.3 Shock-wave thickness

Based on the definition of the shock wave thickness shown in Fig. 3(b), the shock wave thickness  $\delta$  along the stagnation streamline can be obtained from Figs. 4 and 5 for the power-law shapes. As a result of the calculation, Tab. 4 tabulates the shock wave thickness  $\delta$ , normalized by the freestream mean free path  $\lambda_\infty$ , for the cases investigated, and Fig. 6(b) displays the shock wave thickness as a function of the power-law exponent  $n$ .

Table 4: Dimensionless shock wave thickness  $\delta/\lambda_\infty$  for power-law leading edges.

	$n = 1/2$	$n = 2/3$	$n = 3/4$
Diffuse	1.579	0.893	0.650
$\alpha_n = 0.8$	1.657	0.918	0.551
$\alpha_n = 0.6$	1.771	0.950	0.504
$\sigma_i = 0.8$	1.473	0.696	0.396
$\sigma_i = 0.6$	1.364	0.516	0.188

It is evident from Tab. (4) and Fig. 6(b) that the shock wave thickness follows the same trend presented by the shock wave standoff distance in that it decreases with decreasing the tangential accommodation coefficient and increases by a reduction in the normal accommodation coefficient, although the shock thickness decreased slightly for the sharpest leading edge,  $n = 3/4$ , as the normal accommodation coefficient changed from 1 to 0.6.

Again, the circular cylinder provides a much larger shock thickness, i.e.,  $\delta/\lambda_\infty$ , of 3.35, 3.40 and 3.21 for diffuse case,  $\alpha_n = 0.60$  and  $\sigma_i = 0.60$ , respectively. Compared to the power-law shapes, these values are about 2.1, 1.9 and 2.4 times larger than those for power-law exponent of 1/2, respectively.

### 8.4 Shock-wave shape

The shock wave shape, defined by the shock wave center location, is obtained by calculating the position that corresponds to the maximum  $f$  for class III molecules in the  $\eta$ -direction along the body surface (see Fig. 2(b)). The effect of incomplete surface accommodation on the shock wave shape is illustrated in Fig. 7. Figures 7(a) and 7(b) display the shock wave shapes for power-law exponents of 1/2 and 3/4, respectively. In this set of plots,  $X$  and  $Y$  are the cartesian coordinates  $x$  and  $y$  normalized by  $\lambda_\infty$ .

It was pointed out by Lees and Kubota (1957) that when the freestream Mach number  $M_\infty$  is sufficiently large, the hypersonic small-disturbance equations admit similarity solutions for the asymptotic shock wave shapes over power-law bodies, where asymptotic refers to the flowfield at large distances downstream of the nose of the body.

The hypersonic small-disturbance theory states that, for certain exponent  $n$ , a body defined by  $x^n$  produces a shock wave of similar shape and profiles of flow properties transverse to the stream direction that are similar at any axial station not too near the nose. At or near the nose, the surface slope, the curvature, and the higher derivatives are infinite, and

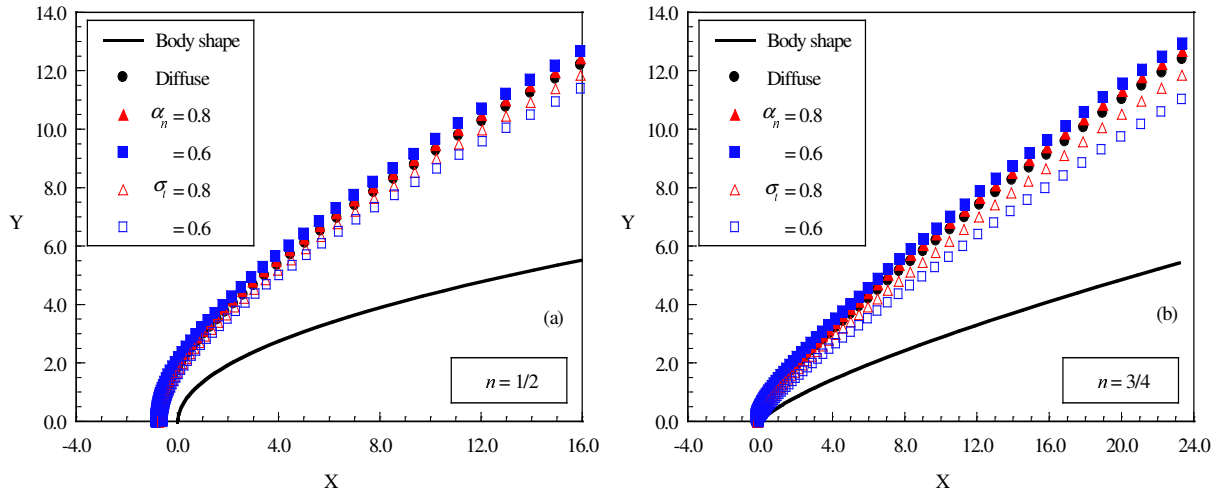


Figure 7: Shock wave shapes on power-law bodies as a function of the surface accommodation coefficient for power-law exponents of (a) 1/2 and (b) 3/4.

the similarity solutions break down. In the more general case for  $0 < n < 1$ , the shock wave grows as  $x^m$ . When  $n$  grows from zero,  $m$  begins by keeping the constant value  $m = 2/3$  for 2-D flow, and if  $n$  keeps on growing towards unity,  $m$  remains equal to  $n$ .

By assuming that power-law bodies generate power-law shock waves in accordance with hypersonic small-disturbance theory (Lees and Kubota, 1957), the shock location coordinates shown in Fig. 7 were used to approximate the shape of the shock wave with a curve fit. A fitting algorithm was performed over these points to approximate the shock shape as a power-law curve of the following form,

$$y = A(x + B)^m \quad (3)$$

where  $A$  is the shock wave power-law constant,  $B$  is the distance from the nose of the leading edge to the shock wave curve fit along the stagnation streamline, and  $m$  is the shock wave power-law exponent.

For comparison purpose,  $A$  and  $B$  in Eq. (3) were found by keeping  $m = 2/3$  for the  $n = 1/2$  case, and  $m = n$  for the  $n = 3/4$  case, where  $n$  and  $m$  stand for body and shock wave power-law exponents, respectively.

It is worthwhile mentioning that the fitting process was performed over the points yielded by DSMC simulations located far from the nose region, say  $X > 3.0$ , where it is expected that the blunt nose effects are not significant. It is also important to recall that the shock wave shape in the vicinity of the nose is not correctly predicted by the theoretical solutions, since the hypersonic slender body approximations are violated close to or at the nose of the leading edges as explained earlier.

Curve fit solutions for shock shape over the power-law exponent of 1/2 are displayed in Figs. 8(a) and 8(b) for normal and tangential accommodation coefficients of 0.6, respectively. In this set of plots, two curve fit solutions are presented: a solution given by keeping  $m = 2/3$ , as predicted by the hypersonic small-disturbance theory, and a curve fit solution obtained by keeping  $m = n = 1/2$ , the body power-law exponent. It is apparent from these figures that the curve fit solutions found for  $m = 2/3$  present an excellent agreement with those solutions provided by the DSMC simulation. In contrast, the curve fit solutions yielded by  $m = n = 1/2$  do not match the shock wave shapes obtained by the DSMC simulation.

Curve fit solutions for shock shape over the power-law exponent of 3/4 are displayed in

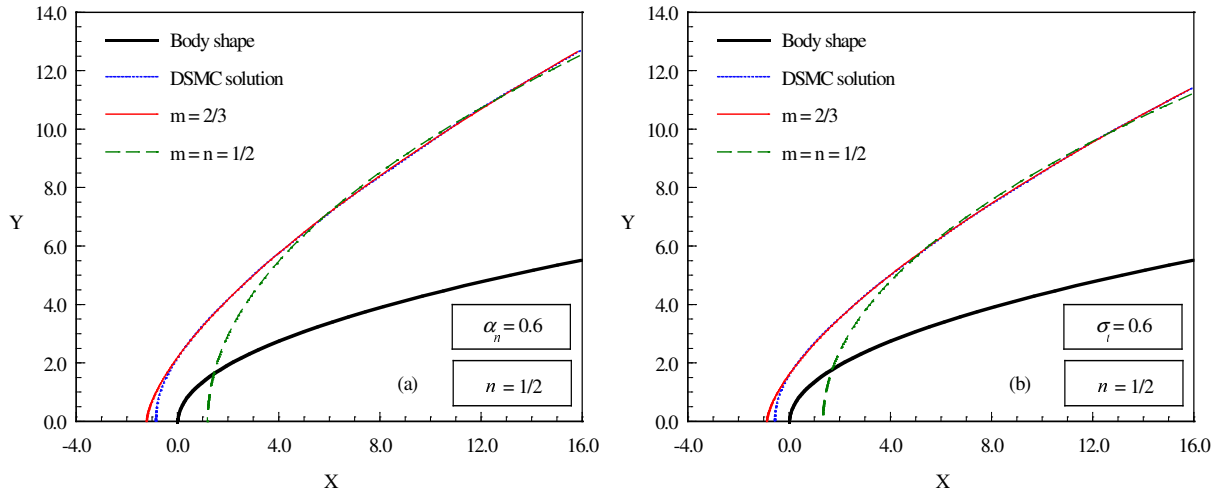


Figure 8: Shock wave shape curve fits on power-law leading edge with power-law exponent of 1/2. (a)  $\alpha_n = 0.6$  and (b)  $\sigma_t = 0.6$ .

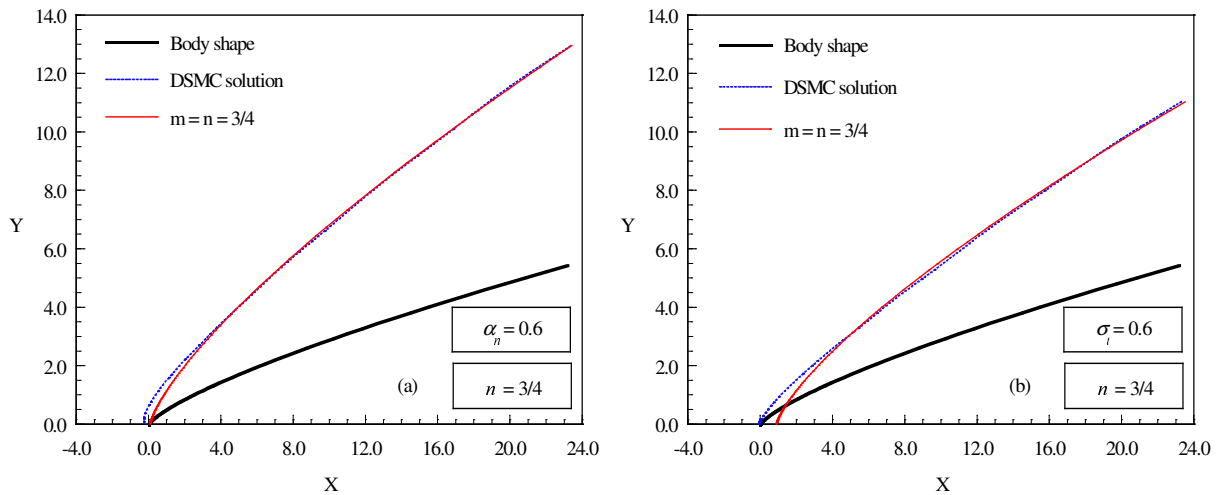


Figure 9: Shock wave shape curve fits on power-law leading edge with power-law exponent of 3/4. (a)  $\alpha_n = 0.6$  and (b)  $\sigma_t = 0.6$ .

Figs. 9(a) and 9(b) for normal and tangential accommodation coefficients of 0.6, respectively. It is clearly seen in these figures that the curve fit solutions given by  $m = n = 3/4$  present good agreement when compared to the shock wave shapes provided by DSMC solution. As a result, the solutions are in qualitative agreement with the Lees and Kubota (1957) findings in the sense that the shock wave shape would follow the shape of the body for body power-law exponent  $n > 2/3$ .

At this point, it should be emphasized that the curve-fitted solutions deviate from the DSMC solution close to the nose of the leading edge, as would be expected. Furthermore, the curve fit exponents are very sensitive to the number of coordinate points used in the fitting process, which define the shock wave center. Certainly, these coordinate points present fluctuations, originated from the DSMC simulations.

## 9. CONCLUDING REMARKS

This study applies the Direct Simulation Monte Carlo method to investigate the shock

wave structure for a family of power-law leading edges. The calculations have provided information concerning the nature of the shock wave detachment distance, shock wave thickness and shock wave shape resulting from variations on the power-law exponent and on the surface accommodation coefficient for the idealized situation of two-dimensional hypersonic rarefied flow.

The analysis showed that the shock wave structure was affected by changes in the normal and tangential accommodation coefficients. It was found that the shock wave standoff and the shock wave thickness increased by a reduction in the normal accommodation coefficient and decreased by a reduction in the tangential accommodation coefficient for the range of the coefficient investigated. In addition, for the power-law bodies investigated, the computational results indicated that the shock wave shape grows with power-law form ( $\propto x^m$ ) far from the nose of the leading edges, as predicted by the hypersonic small-disturbance theory.

## REFERENCES

- Alexander, F. J., Garcia, A. L., & Alder, B. J., 1998, Cell size dependence of transport coefficient in stochastic particle algorithms. *Physics of Fluids*, vol. 10, n. 6, pp. 1540-1542.
- Alexander, F. J., Garcia, A. L., & Alder, B. J., 2000, Erratum: Cell size dependence of transport coefficient is stochastic particle algorithms. *Physics of Fluids*, vol. 12, n. 3, pp. 731-731.
- Anderson, J. L., 1990, Tethered aerothermodynamic research for hypersonic waveriders. *Proceedings of the 1st International Hypersonic Waverider Symposium*, Univ. of Maryland, College Park, MD.
- Bird, G. A., 1981, Monte Carlo simulation in an engineering context. In Sam S. Fisher, ed., *Progress in Astronautics and Aeronautics: Rarefied gas Dynamics*, vol. 74, part I, pp. 239-255, AIAA, New York.
- Bird, G. A., 1989, Perception of numerical method in rarefied gasdynamics. In E. P. Muntz, and D. P. Weaver and D. H. Campbell, eds., *Rarefied gas Dynamics: Theoretical and Computational Techniques*, vol. 118, pp. 374-395, Progress in Astronautics and Aeronautics, AIAA, New York.
- Bird, G. A., 1994, *Molecular Gas Dynamics and the Direct Simulation of Gas Flows*. Oxford University Press, Oxford, England, UK.
- Borgnakke, C. & Larsen, P. S., 1975, Statistical collision model for Monte Carlo simulation of polyatomic gas mixture. *Journal of computational Physics*, vol. 18, n. 4, pp. 405-420.
- Cercignani, C. & Lampis, M., 1971, Kinetic models for gas-surface interactions. *Transport Theory and Statistical Physics*, vol. 1, n. 2, pp. 101-114.
- Garcia, A. L., & Wagner, W., 2000, Time step truncation error in direct simulation Monte Carlo. *Physics of Fluids*, vol. 12, n. 10, pp. 2621-2633.
- Graves, R. E. & Argrow, B. M., 2001, Aerodynamic performance of an osculating-cones waverider at high altitudes. In *35th AIAA Thermophysics Conference*, AIAA Paper 2001-2960, Anaheim, CA.
- Guo, K. & Liaw, G.-S., 2001, A review: boundary conditions for the DSMC method. In *Proceedings of the 35th AIAA Thermophysics Conference*, AIAA Paper 2001-2953, Anaheim, CA.
- Hadjiconstantinou, N. G., 2000, Analysis of discretization in the direct simulation Monte Carlo. *Physics of Fluids*, vol. 12, n. 10, pp. 2634-2638.
- Lees, L. & Kubota, T., 1957, Inviscid hypersonic flow over blunt-nosed slender bodies. *Journal of Aeronautical Sciences*, vol. 24, n. 3, pp. 195-202.

- Lord, R. G., 1991a, Application of the Cercignani-Lampis scattering kernel to direct simulation Monte Carlo method. In A. E. Beylich, ed., *Proceedings of the 17th International Symposium on Rarefied Gas Dynamics*, pp. 1427-1433, Aachen, Germany.
- Lord, R. G., 1991b, Some extensions to the Cercignani-Lampis gas-surface scattering kernel. *Physics of Fluids*, vol. A3, n. 4, pp. 706-710.
- Lord, R. G., 1995, Some further extensions of the Cercignani-Lampis gas-surface interaction model. *Physics of Fluids*, vol. 7, n. 5, pp. 1159-1161.
- Mason, W. H. & Lee, J., 1994, Aerodynamically blunt and sharp bodies. *Journal of Spacecraft and Rockets*, vol. 31, n. 3, pp. 378-382.
- Maxwell, J. C., 1879, On stresses in rarefied gases arising from inequalities of temperature. *Philosophical Transactions of the Royal Society of London*, vol. 170, Pt. 1, pp. 231-256, reprinted in *The Scientific Papers of J. C. Maxwell*, Dover, New York, 1965.
- Nonweiler, T. R. F., 1959, Aerodynamic problems of manned space vehicles. *Journal of the Royal Aeronautical Society*, vol. 63, Sept, pp. 521-528.
- Potter, J. L. & Rockaway, J. K., 1994, Aerodynamic optimization for hypersonic flight at very high altitudes. In B. D. Shizgal and D. P. Weaver, eds., *Rarefied gas Dynamics: Space Science and Engineering*, vol. 160, pp. 296-307, Progress in Astronautics and Aeronautics, AIAA New York.
- Rault, D. F. G., 1994, Aerodynamic characteristics of a hypersonic viscous optimized waverider at high altitude. *Journal of Spacecraft and Rockets*, vol. 31, n. 5, pp. 719-727.
- Santos, W. F. N. & Lewis, M. J., 2002a, Power law shaped leading edges in rarefied hypersonic flow. *Journal of Spacecraft and Rockets*, vol. 39, n. 6, pp. 917-925.
- Santos, W. F. N. & Lewis, M. J., 2002b, Angle of attack effect on rarefied hypersonic flow over power law shaped leading edges. In *23rd International Symposium on Rarefied Gas Dynamics*, Whistler, BC, Canada.
- Santos, W. F. N. & Lewis, M. J., 2003, Aerodynamic heating performance of power law leading edges in rarefied hypersonic flow. In *36th AIAA Thermophysics Conference*, AIAA Paper 2003--3894, Orlando, FL.
- Santos, W. F. N. & Lewis, M. J., 2004a, Effects of compressibility on rarefied hypersonic flow over power law leading edges. In *42nd AIAA Aerospace Sciences Meeting and Exhibit*, AIAA Paper 2004-1181, Reno, NV.
- Santos, W. F. N. & Lewis, M. J., 2004b, DSMC calculations of rarefied hypersonic flow over power law leading edges with incomplete surface accommodation. In *34th AIAA Fluid Dynamics Conference and Exhibit*, AIAA Paper 2004-2636, Portland, OR.
- Santos, W. F. N. & Lewis, M. J., 2005, Calculation of shock wave structure over power-law bodies in hypersonic flow. *Journal of Spacecraft and Rockets*, vol. 42, n. 2, pp. 213-222.
- Santos, W. F. N., 2004a, Shock wave shape on power-law leading edges. In *24th International Symposium on Shock Waves*, Beijing, China.
- Santos, W. F. N., 2004b, Power-law shapes for leading-edge blunting with minimal standoff distance in low-density hypersonic flow. In *24th International Symposium on Shock Waves*, Beijing, China.
- Santos, W. F. N., 2005, Leading-edge bluntness effects on aerodynamic heating and drag of power-law body in low-density hypersonic flow. *Journal of Brazilian Society of Mechanical Sciences and Engineering*, vol. XXVII, n. 3, pp. 236-241 (in press, to appear).
- Schaff, S. and Chambre P., 1958, *Fundamentals of Gas Dynamics*. Princeton University Press, Princeton, NJ.
- Shvets, A. I., Voronin, V. I., Blankson, I. M., Khikine, V., & Thomas, L., 2005, On waverider performance with hypersonic flight speed and high altitudes. *43rd AIAA Aerospace Sciences Meeting and Exhibit*, AIAA Paper 2005-0512, Reno, NV.